Numerical investigation of roughness effect on wet steam ejector performance in the refrigeration cycle

Rad Mehdi Poyan, Lakzian Esmail, Grönman Aki

DOI: 10.1007/s00231-022-03197-z

Numerical investigation of roughness effect on wet steam ejector performance in the refrigeration cycle

Mehdi Pouyan Rad [a], Esmail Lakzian [a,*], Aki Grönman[b]

[a] *Center of Computational Energy, Department of Mechanical Engineering, Hakim Sabzevari University, Sabzevar, Iran*

[b] *LUT University, School of Energy Systems, Yliopistonkatu 34, P.O. Box 20, 53851, Lappeenranta, Finland*

** Corresponding author: e.lakzian@hsu.ac.ir, Tel: +98 51 4401 28 18 / Fax: +98 51 4401 2773*

Abstract

Machining operation and presence of water droplet cause increasing the surface roughness of wet steam ejector walls and changing its performance in the refrigeration cycle. The purpose of this work is to investigate the influences of the primary nozzle surface roughness on wet steam ejectors in the refrigeration cycle with steam water as a working flow. The flow is modeled by solving governed equations based on the Eulerian-Eulerian approach. The proposed model is validated by comparison numerical results with experimental data of the ejector and nozzle. Moreover, different surface roughness has been successfully applied to the primary nozzle and its effect on the entire flow is shown. Six properties of wet steam are selected, including pressure, temperature, Mach number, droplet average radius, droplet growth rate, and liquid mass fraction. The result shows, increase in the surface roughness resulted in a shift of the shock chain to the primary nozzle, damping shock strength, and increasing temperature in the diffuser. In addition, increment of the primary nozzle surface roughness decreases ER and COP of the refrigeration cycle by 3.67% and 3.8%, respectively. According to the important impact of the roughness on the liquid mass fraction, droplet average radius, droplet growth rate, ER, and COP, designers and operators should be considered the roughness effects in the design and operation of wet steam ejectors.

Key Words: wet steam ejector, roughness, refrigeration cycle, Entrainment Ratio, COP

Nomenclatures

D_ω	cross-diffusion term(kgm^{-1} s^{-3})
E	total energy (J)
ER	entrainment ratio (-)
f_r	roughness function (-)
G	Gibbs free energy (J kg^{-1})
$\tilde{G}_k$	turbulence kinetic energy generation (kgm^{-1} s^{-3})
G_ω	generation of ω(kgm^{-1} s^{-3})
h	enthalpy (J kg^{-1})
J	nucleation rate (m^{-3} s^{-1})
k	turbulent dissipation rate (m^2 s^{-3})
K_s^+	non-dimensional roughness height
Y_k	dissipation of k (kgm^{-1} s^{-3})
Y_ω	dissipation of ω (kgm^{-1} s^{-3})
y^+	dimensionless wall distance

Greek symbols

α	thermal conductivity (W m^{-1} K^{-1})
β	liquid mass fraction (-)
Γ	mass generation rate (kg m^{-3} s^{-1})
δij	rate of mixing layer growth (-)
η	number of droplets (m^{-3})
μ	dynamic viscosity (Pa s)
ρ	density (kg m^{-3})

k_s	physical roughness height (m)
K_B	Boltzmann's constant
L	nozzle length(m)
m	mass of one molecule (mg)
$\dot{m}$	mass flow rate (kg s^{-1})
Ma	Mach number
P	pressure (Pa)
$\dot{Q}$	rate of heat exchange (W m^{-2} s^{-1})
q_c	condensation coefficient (-)
r_*	critical radius of droplets (μm)
r	droplet radius (μm)
$\dot{r}$	droplet growth rate (μm s^{-1})
R	gas constant ($JK^{-1}mol^{-1}$)
S	saturation ratio (-)
S_k	source terms of ω (kgm^{-1} s^{-3})
S_ω	source terms of ω (kgm^{-1} s^{-3})
T	temperature (K)
u	velocity (m s^{-1})
V_d	mean volume of the droplets (m^3)
x	spatial component (m)
σ	liquid surface tension (N m^{-1})
σ_k	indicate turbulent Prandtl numbers for k
σ_ω	turbulent Prandtl numbers for ω
τ	stress tensor (Pa)
ω	specific turbulence dissipation (s^{-1})

subscribes

s	secondary
p	primary
e	exit
g	gas (vapor)
eff	effective
l	liquid
v	vapor

Abbreviation

PNE	Primary Nozzle Exit

Math symbols

-	average

1. Introduction

A wide range of application, simple structure, energy-saving, and reducing environmental pollution, has made ejectors as attractive equipment for researchers as well as industrial equipment manufacturers. Vast numerical and experimental studies performed in recent decades can help the manufacturers of this equipment to upgrade their products for future systems. On the other hand, besides the machining operation, the presence of high pressure, high velocity, and sometimes corrosive gases, and liquids cause corrosion/erosion of the ejector surfaces, which means increasing the surface roughness and changing in ejector performance during operation. Corrosion/erosion may be more evident in wet steam ejectors due to the presence of high-speed condensed droplets that hit the inner surface of the ejector and makes it rough. Therefore, surface roughness can play a major role in the operation of ejectors.

Various experimental and numerical studies have been published in the field of wet steam in nozzles and blades. The Eulerian-Eulerian approach with two methods of density-based and pressure-based can be used for modeling wet steam flow in fluent. Both methods have good similarities against experimental data [1]. Yazdani and Lakzian [2] applied the Eulerian-Lagrangian model to shows the effect of impressing holes in the pressure and suction side of the blade on the performance of the steam turbine. They presented complete elimination of wetness

when the inlet of holes are closer to the leading edge of the pressure and suction side. Condensed droplets in wet steam can be considered as monodispersed or polydispersed models. These two models have been simulated in a recent paper by Ding et al. [3] using exergy analysis and polydispersed model that shows more accurate results rather than the monodispersed model. In both of mono and polydispersed model, two-phase flow can be considered as single-fluid or two-fluid, but two-fluid model can predict thermodynamic loss and indicates better agreement in droplet radius and drag forces with experimental data [4]. Particle Image Velocimetry (PIV) method was applied for the investigation of polydispersed condensing flow [5]. In a different method, impulse facility techniques with the aid of image post-processing tools can show several phenomena that occurred in nozzles. Among them, shock waves and condensation can be seen easily [6]. As mentioned previously, wet steam studies can be extended to more complex but similar geometries of the ejectors.

Although the focus of this study is on water wet steam, in the general view, various fluids are used in ejectors based on their application including water, air and, refrigerants. In refrigeration application, a comparison between 10 different fluids for ejector chillers shows that water has good performance but the assumption of steam as ideal gas is not appropriate in the simulation of flow in wet steam ejector [7]. Condensation creates a two-phase flow that wet steam solution gives more accurate results and improves the performance parameters of ejectors [8]. In addition to condensation that prevalently occurs in the primary nozzle, the results obtained by Faghih et al.[9] indicated that existence of droplet in motive flow postpones condensing shock and reduce motive and suction mas flow as well as entrainment ratio (ER). Furthermore, it is observed that reduction in the wetness of suction flow can increase ER as well as system performance [10]. In another work, a modified nucleation model by Zhang et al. [11] predicted a reduction in ER in the critical zone and increasing in critical zone length. On the other hand, reduction or elimination of condensation can help to the improvement of ejector performance. It has been proved that an increase in the degree of superheat in the primary inlet causes a delay in the location of nucleation and reduction of the intensity of the condensation shock [12] and increment of ER [13]. Nucleation is one of the main factors in the growth of the mixing layer between the primary and secondary flow. Ariafar et al. [14] argued that under a fixed condition for the primary and discharge, the mixing layer has maximum effect on ER at lower secondary pressure.

Similar to other scientific researches, experimental data were used as the main reference for validating the results in the ejectors. Obtained data by modern technic and advanced instrument on ejectors as well as convergent-divergent nozzles reveal several unseen phenomena can conduct theoretical research into true path. Tang et al. [15] represented results of experimental setup that show the ununiformed distribution of droplets in each cross-section and increase of condensate quantity with entrainment ratio. In addition, Rayleigh scattering of the supersonic condensing jet flow and reverse condensing flows are photographed and observed phenomena are discussed. On another experimental study in critical pressure condition, the result showed the starting main shock waves occurs between mixing chamber and fixed area section [16].

In addition to the two-phase behavior of flow, one of the other parameters that researchers have addressed is the geometry of the ejector. Entropy generation, ER, critical compression ratio, and COP of refrigeration system are used by Foroozesh et al. [17] to modify the geometry of the ejector. The new design improves ER and critical compression ratio by 32%. Dong et al. [18] examined the effect of mixing chamber on performance, considering deferent Mach number at the exit of the primary nozzle and length of fixed area section and diffuser. Zhang et al. [19] reported that Genetic algorithm optimization of the primary nozzle geometry using modified nucleation model based Benson surface tension increases the ER of ejector approximately 27%.

Some of other researchers have addressed the issue of the surface roughness along with extra parameters. An increase in area ratio between the primary nozzle exit and throat reduces nozzle outlet pressure and condensation intensity and increases liquid mass fraction. Besides, increase in surface roughness causes reduction in mass flow rate and increases in dryness [20]. Mahmoudian et al. [21] tested a prototype ejector chiller with R134a working refrigerant and briefly mentioned that the ejector with smooth surface has higher performance. Energy loss is directly related to surface roughness in each part of ejectors with ideal gas as a working flow but among them, diffuser surface roughness has a maximum impact [22]. Roughness values from 5μ to 300μ were investigated for the inner surface of the ejector by Zhang et al. [23]. Their results showed an increase in temperature and a reduction in the performance of the ejector. Wang et al. [24] took into account friction on the throat, using the modified law of the wall and indicated reduction of entrainment of the ejector due to increase in roughness. In fact, roughness acts like reverse pressure and displaces the shock waves to upstream [25].

Researches demonstrate similar results in the investigation of roughness in blades and nozzles. In the study of Laval nozzle, Pillai and Prasad [26] indicated that condensation shock strength is adjusted due to increasing roughness, but the thickness of the boundary layer increases. Han et al. [27] argued that increase in surface roughness, decreases Mach number and peak of nucleation rate in the turbine blade. In addition, Ding et al. [28] have demonstrated that increase in average height of sand-grain roughness causes entropy generation growth. Investigations show more performance loss in the subsonic region with comparison of supersonic in turbine blades [29].

Even though several studies in the literature have been performed on the subject of roughness in ejectors, but no researchers have addressed the effect of surface roughness on the ejector with water steam as a working fluid in the refrigeration cycle. Nonetheless, it is possible to investigate the impact of surface roughness on wet steam properties. Therefore in this paper, we would like to present a comprehensive study which is carried out in detail and has taken into account the effect of the primary surface roughness in such flows. These results are presented for the first time in the field of wet flow with water steam as working fluid.

2. Problem definition

Fig.1A shows the schematic diagram of the studied ejector with rough walls. For a better understanding of the issue, a simple schematic of wall roughness has been magnified in this figure. The ejector consists of the primary nozzle, suction cup, mixing chamber, constant area, and diffuser. Water steam is expanded in the primary nozzle and caused a sharp drop in temperature and pressure. Under certain condition, the steam passes through the saturation line and rapidly enter to the two-phase region. In this condition, steam is non-equilibrium and expands continually up to Wilson Line, where in terms of thermodynamic the steam is super-cooled. Increase in degree of supercooling and in the absence of external surfaces, the homogeneous nucleation occurs. This phenomenon is known as condensation shock.

Moreover, steam expansion continues in the mixing chamber which is caused the pressure drops to the minimum value. Therefore, the secondary flow sucked into the ejector. These two streams are mixed and then enter the constant area. From the outlet of the primary nozzle to the beginning of diffuser, the pressure fluctuates and forms the shock chain. Then, it increases gradually to the outlet of the ejector. In the present study, wet steam flow in the ejector with different primary nozzle surface roughness is numerically analyzed. The ejector of refrigeration cycle developed by

Ruangtrakoon et al. [30] was selected as a case study (Fig 1B). In mentioned cycle, the total temperature and total pressure at the primary are 270kPa and 403K, respectively. Further, total temperature and total pressure at suction are 283K and 1.228kPa and outlet flow are, 300K and 4kPa, respectively. Note that, it is assumed the inner surface of the wall ejector is adiabatic.

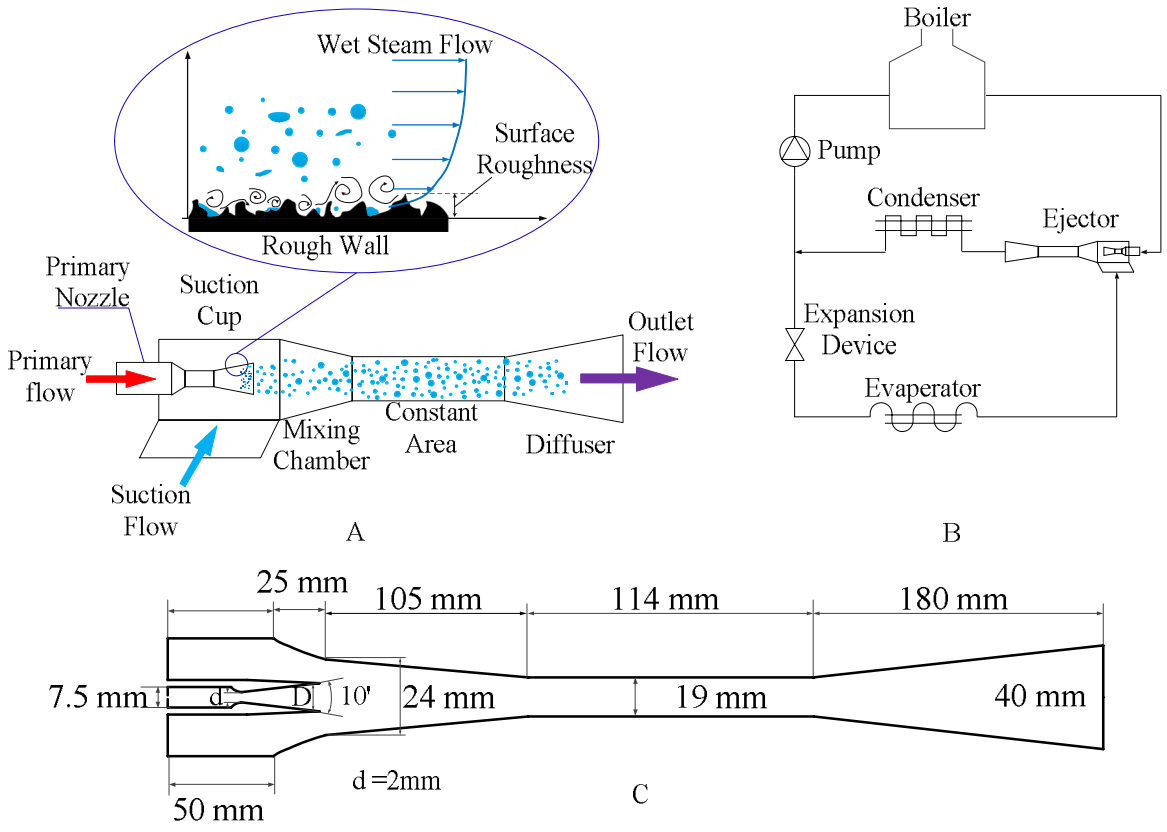

Fig.1. Schematic of A) wet steam ejector and surface roughness in the primary nozzle, B) water refrigeration cycle, and C) dimensions of the ejector

The performance of the ejectors in the refrigeration cycle can be indicated by two key parameters of ER and COP as follows [17]:

$$ER = \frac{\dot{m}_s}{\dot{m}_p} \tag{1}$$

$$COP = \frac{\dot{Q}_{evap}}{\dot{Q}_{boiler}} = \frac{\dot{m}_s(h_{g(T_{evap})} - h_{f(T_{cond})})}{\dot{m}_p(h_{g(T_{boiler})} - h_{g(T_{evap})})} = ER\frac{\Delta h_{evap}}{\Delta h_{boiler}} \tag{2}$$

3. Mathematical modeling

3.1. Governing equations

The steady state compressible Navier-Stokes equations applied for mixture flow including continuum, momentum, and energy equation. These three equations can be simplified and written as follows:

$$\frac{\partial}{\partial x_i}(\rho u_i) = 0 \tag{3}$$

$$\frac{\partial}{\partial x_j}\left(\rho u_i u_j\right) = -\frac{\partial P}{\partial x_i} + \frac{\partial \tau_{ij}}{\partial x_j} \tag{4}$$

$$\frac{\partial}{\partial x_i}(u_i(\rho E + P)) = \frac{\partial}{\partial x_i}(\alpha_{eff}\frac{\partial T}{\partial x_i}) + \frac{\partial}{\partial x_i}(u_i \tau_{ij}) \tag{5}$$

where, $\rho, u, P, E,\ T, and\ \alpha_{eff}$ are mixture density, velocity, pressure, total energy, temperature, and, thermal conductivity, respectively [5]. τ_{ij} is viscous shear stress tensor and expressed as following:

$$\tau_{ij} = \mu_{eff}\left(\frac{\partial u_i}{\partial x_j} + \frac{\partial u_j}{\partial x_i}\right) - \frac{2}{3}\mu_{eff}\frac{\partial u_k}{\partial x_k}\delta_{ij} \tag{6}$$

where μ_{eff} and δ_{ij} are dynamic viscosity and mixture layer growth rate. The virial third-order state equation that describes the relation of pressure, temperature, and vapor density (ρ_v) is as follows:

$$P = \rho_v RT(1 + B\rho_v + C{\rho_v}^2) \tag{7}$$

where B and C are coefficients and can be found in thermodynamic references. Density of vapor ρ_v in state equation can be related to the density of mixture ρ in Navier-Stokes equations as follows:

$$\rho = \frac{\rho_v}{(1-\beta)} \tag{8}$$

where β denotes liquid mass fraction. Some basic assumptions for modeling wet steam as following [31]:

- Vapor is continuous phase.
- The droplets are spherical-shaped.
- There is zero relative velocity between vapor and liquid phases.

- Liquid phase volume and interaction between droplets are negligible.
- liquid mass fraction is 0.2 or less
- The minimum temperature of flow in this problem is 273.15K.

Modeling non-equilibrium condensation needs two additional transport equations. These equations are transporting equation of liquid mass fraction (Eq.(9)) and number density of droplet (Eq.(10)) and can be defined as below [11]:

$$\frac{\partial(\rho\beta)}{\partial t} + \frac{\partial}{\partial x_i}(\rho\, u_i\, \beta) = \Gamma \tag{9}$$

$$\frac{\partial \rho\eta}{\partial t} + \frac{\partial}{\partial x_i}(\rho\, u_i\, \eta) = \rho J \tag{10}$$

where Γ is the rate of liquid mass generation due to exchanging between liquid and vapor phase and J is droplet nucleation rate per unit volume. η shows the number of droplets per unit volume. The following relation is used for the calculation of these three parameters:

$$\Gamma = \frac{3}{4}\pi\rho_l I r_*^3 + 4\pi\rho_l\eta\bar{r}^2\frac{\partial\bar{r}}{\partial t} \tag{11}$$

$$J = \frac{q_c}{1+\theta}\left(\frac{\rho_v^2}{\rho_l}\right)\sqrt{\frac{2\sigma}{M_m^3\pi}}\exp\left(-\frac{4\pi r_*^2\sigma}{3k_B T}\right) \tag{12}$$

$$\eta = \frac{\beta}{(1-\beta)V_d\left(\frac{\rho_l}{\rho_v}\right)} \tag{13}$$

The function r_* is critical droplet radius that derived from Gibbs free energy equation under the condition of the stability of the droplet:

$$r_* = \frac{2\sigma}{\rho_l R T_v \ln Sr} \tag{14}$$

where σ is calculated liquid surface tension at T and ρ_l is density of the condensed liquid. $\frac{\partial\bar{r}}{\partial t}$ denotes the rate of droplet volume change due to the growth of existing droplets:

$$\frac{\partial\bar{r}}{\partial t} = \frac{p}{h_{lv}\rho_l\sqrt{2\pi RT}}\frac{C_p + C_v}{2}\left(T_s(p_v) - T_v\right) \tag{15}$$

where $[T_s(p_v) - T_v]$ denote degree of supercooling and θ is Kantrowitz non-isothermal correction which calculated as follows:

$$\theta = 2\frac{\gamma-1}{\gamma+1}\frac{h_{lv}}{RT_v}\left(\frac{h_{lv}}{RT_v}-\frac{1}{2}\right) \tag{16}$$

By the assumption of the spherical form of droplets, the mean volume of the droplets is defined as:

$$V_d = \frac{4}{3}\pi\bar{r}^3 \tag{17}$$

3.2. Law-of-the-Wall Modified for Roughness

Eq.(18) shows the logarithmic profile of mean velocity used to take into account of surface roughness effect:

$$\frac{u_p u^*}{\tau_w/\rho} = \frac{1}{\kappa}\ln\left(\frac{\rho u^* y_p}{\mu}\right) - \Delta B \tag{18}$$

where u_p is the velocity at the cell near wall and u^* the wall friction velocity which can be defined as:

$$u^* = C_\mu^{1/4} k^{1/2} \tag{19}$$

$$\Delta B = \frac{1}{\kappa}\ln(f_r) \tag{20}$$

$$K_s^+ = \rho k_s u^*/\mu \tag{21}$$

$$\Delta B = \begin{cases} 0 & K_s^+ \le 2.25 \\ \frac{1}{\kappa}\ln\left[\frac{K_s^+ - 2.25}{87.75} + C_s K_s^+\right] \times \sin[0.4258(\ln K_s^+ - 0.811)] & 2.25 \le K_s^+ \le 90 \\ \frac{1}{\kappa}\ln(1 + K_s^+) & K_s^+ \ge 90 \end{cases} \tag{22}$$

where f_r, K_s^+, k_s, and C_s are roughness function, nondimensional roughness height, physical roughness height, and roughness constant, respectively. Moreover, ΔB depends on the type and size of the wall roughness that shows three equations for hydro-dynamically smooth, transitional, and fully rough surface.

3.3. Turbulent model

The $SST\ k-\omega$ turbulent model is selected in the present work. The SST k-ω turbulence model is good to capture the condensation shock in high speed compressible ejector in wet steam flow.

Furthermore, this model has good agreement with experimental data [32] and predict shocks. This model can be expressed by the following equations:

$$\frac{\partial(\rho k)}{\partial t} + \frac{\partial(\rho k u_i)}{\partial x_i} = \frac{\partial}{\partial x_j}\left(\left(\mu + \frac{\mu_t}{\sigma_k}\right)\frac{\partial k}{\partial x_j}\right) + \tilde{G}_k - Y_k + S_k \quad (23)$$

$$\frac{\partial(\rho \omega)}{\partial t} + \frac{\partial(\rho \omega u_i)}{\partial x_i} = \frac{\partial}{\partial x_j}\left(\left(\mu + \frac{\mu_t}{\sigma_\omega}\right)\frac{\partial \omega}{\partial x_j}\right) + G_\omega - Y_\omega + D_\omega + S_\omega \quad (24)$$

where $\tilde{G}_k$, G_ω , D_ω , $Y_k, and\ Y_\omega$ are turbulence kinetic energy generation because of the mean velocity gradients, generation of ω, the cross-diffusion term, dissipation of k due to turbulence, and dissipation of ω due to turbulence, respectively. Also, σ_k and σ_ω indicate turbulent Prandtl numbers for k and ω. In $SST\ k-\omega$ turbulence model, S_k and S_ω denote source terms.

3.4. Area-weighted average

The area-weighted average of a sample quantity of X is obtained by dividing the summation of the product of the selected field variable and facet area by the total area of the surface as following:

$$\bar{X} = \frac{1}{A}\int X dA \quad 25$$

4. Result and discussion

In the present study, numerical modeling performed using CFD software for compressible 2D axisymmetric flow. The value of 1×10^{-6} for the relative residual of all dependent variables considered as the convergence criterion. To validate the purposed approach and indicate its reliability, before applying it for the flow throughout the ejector, the approach is used to simulate non-equilibrium wet-steam flow in Moore B nozzle.

4.1. Nozzle

4.1.1. Independency and validation

Type and number of cells can accelerate convergence and can rise solution accuracy. Therefore, to achieve minimum cell with maximum solution accuracy, mesh independence and choosing the optimum grid is necessary. In this paper, first, the mesh independence is investigated in Moore B nozzle. Coordinates and boundary conditions of this nozzle are given in Table.1. Five meshes with

$20 \times 100, 30 \times 150, 40 \times 200, 50 \times 250$, and 60×300 cells, using structured mesh are applied. Fig.2A indicates a clear view of the nozzle mesh domain. Fig.2B shows liquid mass fraction (β) in nozzle exit for these five meshes. As can be seen, β increases as the number of cells increases. But, these changes become insignificant for mesh with more than 50×250 cells. Therefore, this mesh is selected as the optimum grid. The concentration of grids increases in the throat and near walls where the gradients are important.

Table.1. Coordinates and boundary conditions of Moore B nozzle

Moore B Nozzle	Boundary condition [P (kPa) , T (K)]	Coordinate [x(m), y(m)]
Inlet	[25, 357.6]	[-0.25, 0.056] [-0.25, -0.056]
Outlet	[6, 310]	[0.5, 0.072] [0.5, -0.072]

Wet steam flow is simulated for the Moore B nozzle. Fig.2C shows the comparison of droplet radius (r) and static pressure measurement with their values of the experimental test [33, 34]. Acceptable accuracy in results and good agreement with experimental data indicate the appropriated mesh and choosing suitable procedure in problem simulation.

4.1.2. Effect of roughness on flow in the nozzle

Fig.3(A) indicates the nozzle mass flow rate by increasing the surface roughness. Five cases of the average roughness height (k_s) have been considered including; 0μm (smooth), $30\mu m$, $100\mu m$, $300\mu m$ and $1000\mu m$. It is evident that the growth of roughness height from 0 to $1000\mu m$ reduces the mass flow rate by 1%.

Fig. 3(B) presents the profiles of the pressure for five different surface roughness values. In all five cases, the inlet and outlet condition maintain at 25kPa and 6kPa, respectively. It is found that the pressure increases by increasing the roughness. In addition, the roughness delays the condensation shock, and therefore, this shock occurs at a greater distance after the throat.

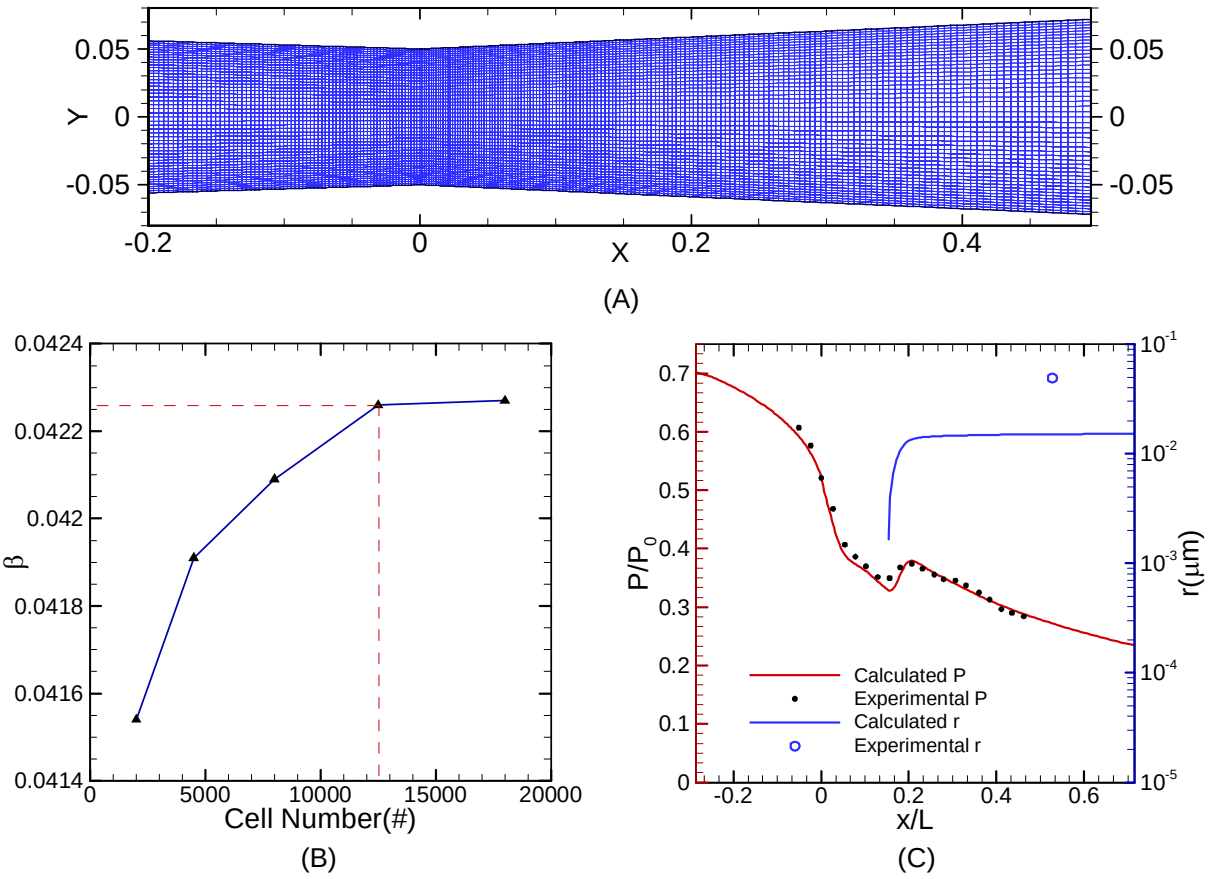

230

231 **Fig.2. A) nozzle geometry and mesh, B) mesh independence, and C) solution validation**

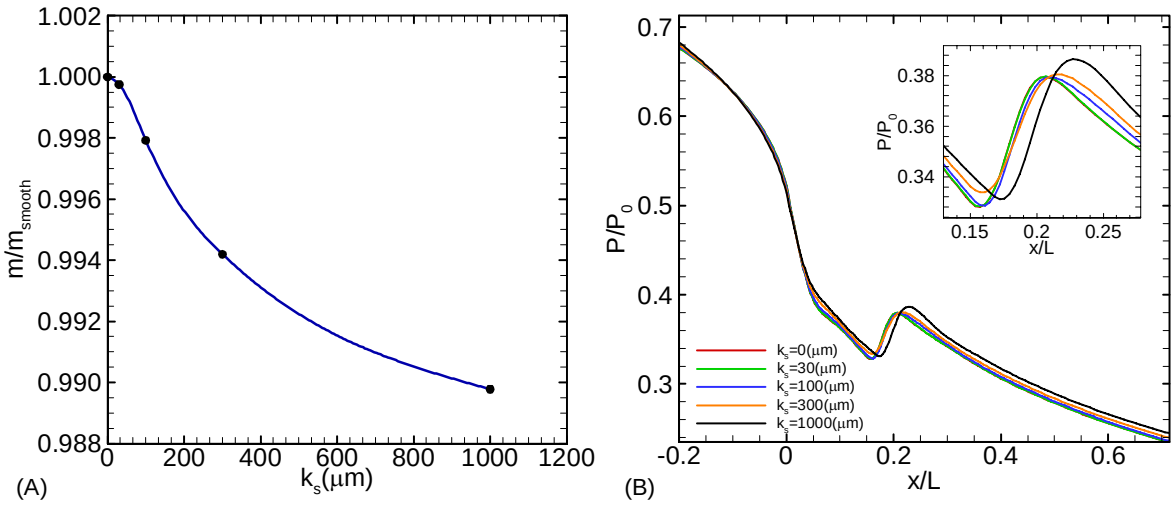

232

233 **Fig.3. Effect of roughness height on A) mass flow rate and B) pressure of wet steam nozzle**

234

4.2. Ejector

4.2.1. Independency and validation

Fig.4A shows the geometry and mesh grid for the proposed ejector. To evaluate the impact of roughness on flow, the boundary layer mesh must be applied. Therefore, as can be seen in the magnified zone of the primary nozzle, the near-wall mesh is finer than elsewhere. Similar to the nozzle, mesh independence for the ejector is performed. For this purpose, three different densities of the structural grids including 50000, 125000, and 200000 cells are applied to check the grid independence. The static pressure is selected as a parameter of the test of grids. As can be seen in Fig.4B, there is no significant variation in pressure for mesh with more than 125000 cells. Therefore, this mesh is chosen as the best mesh for the simulation of wet steam.

The ER for different back pressure is employed to validate the numerical model. Consider Fig.4C, which plots ER for wet and dry ejector in comparison with experimental data [30] in different backpressure. As shown, ER is approximately constant until the backpressure reaches critical pressure where ER drops down. For the pressure value more than critical point, ER decreases and tends to zero as well as backpressure increase. This diagram can give an overview of the ejector performance at different pressure. The results are very similar to the results obtained by experimental test which can emphasize the validity of used model.

4.2.2. Effect of the primary nozzle surface roughness on wet steam properties

The wet steam ejector is simulated using the CFD model in six different surface roughness height for the primary nozzle including; $0\mu m$ (smooth), $20\mu m$, $40\mu m$, $80\mu m$, $160\mu m$, and $320\mu m$. It should be mentioned that, in this problem, rough surface creates by three reasons, which are: (I) intrinsic surface roughness, (II) machining process, and (III) corrosion and erosion due to high-velocity flow and collision of condensed droplets with the nozzle wall. To show the effects of the primary nozzle surface roughness, six properties of wet steam are selected due to their importance of them in numerical studies, including pressure, temperature, Mach number, droplet average radius (r), droplet growth rate ($\dot{r}$), and liquid mass fraction (β).

Investigating compressible flow in the supersonic adiabatic nozzle shows that three main factors affect the flow including; cross-section area changes, heat transfer due to non-equilibrium condensation, and friction (see Fig.5). It should be noted that simultaneous examination of these

factors complicates the issue due to the complex relation between properties, however, they can be examined separately.

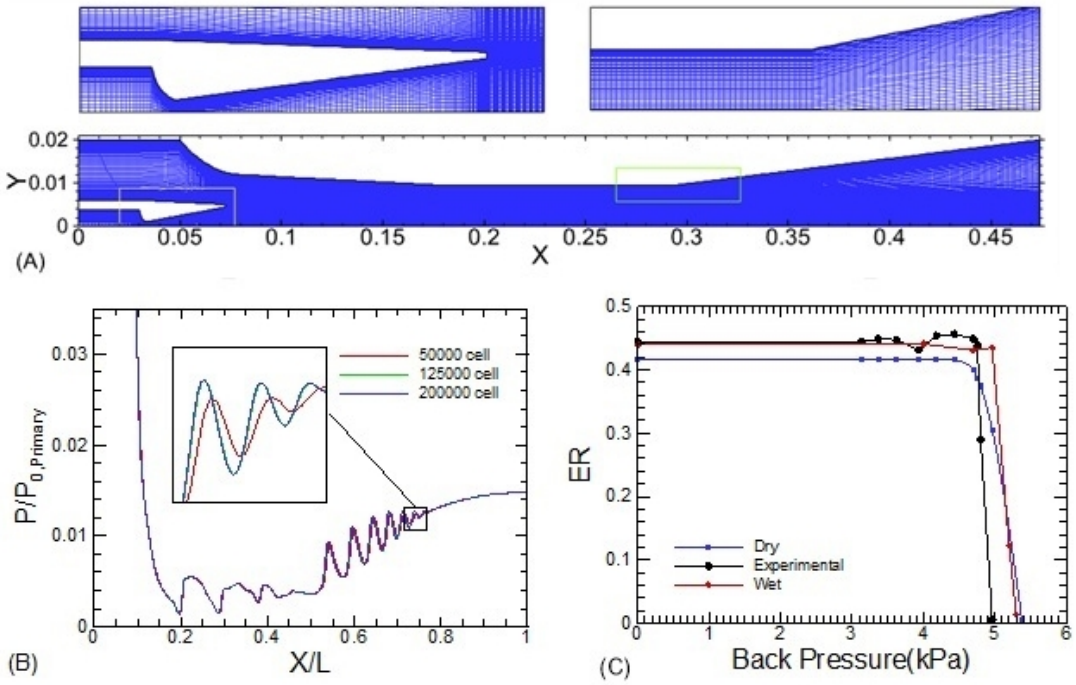

Fig.4. A) ejector geometry and mesh B) mesh independency, and C) validation

The first important factor in supersonic primary nozzle study is area change which means expansion of the vapor. The expansion rate of the primary nozzle is related to the nozzle exit diameter. This diameter can vary the secondary mass flow rate in the ejector problem. It can be seen that the high expansion rate along the primary nozzle occurs due to increase in cross-section area (Fig.5B). This is completely in agreement with dynamic behavior of compressible adiabatic vapor through a diffuser when flow is supersonic [35]. Nozzle flows start from dry saturated state and expand up to Wilson Line where the maximum supercooling occurs. At this point, nucleation occurs and temperature and pressure rise due to latent heat transfer from water droplet to steam. Next, steam expansion continues up to the nozzle outlet. As a result, the maximum variation in temperature is due to area change in the primary nozzle compare to latent heat and friction effects.

Latent heat transfer due to non-equilibrium condensation is the second factor which is the predominant phenomenon at $\frac{x}{L} = 0.07$ to $\frac{x}{L} = 0.08$ in the primary nozzle (see Fig.5C). This position can be distinguished as a sudden jump in droplet average radius. Increment in droplets

radius means more latent heat transition to the steam phase. The heat is released during the condensation from the droplets to steam which causes a rise of the static temperature downstream the primary nozzle throat. Therefore, the flow returns to the thermodynamic equilibrium conditions. The consequence of this heat transfer is reduction in nucleation rate and steam subcooling levels.

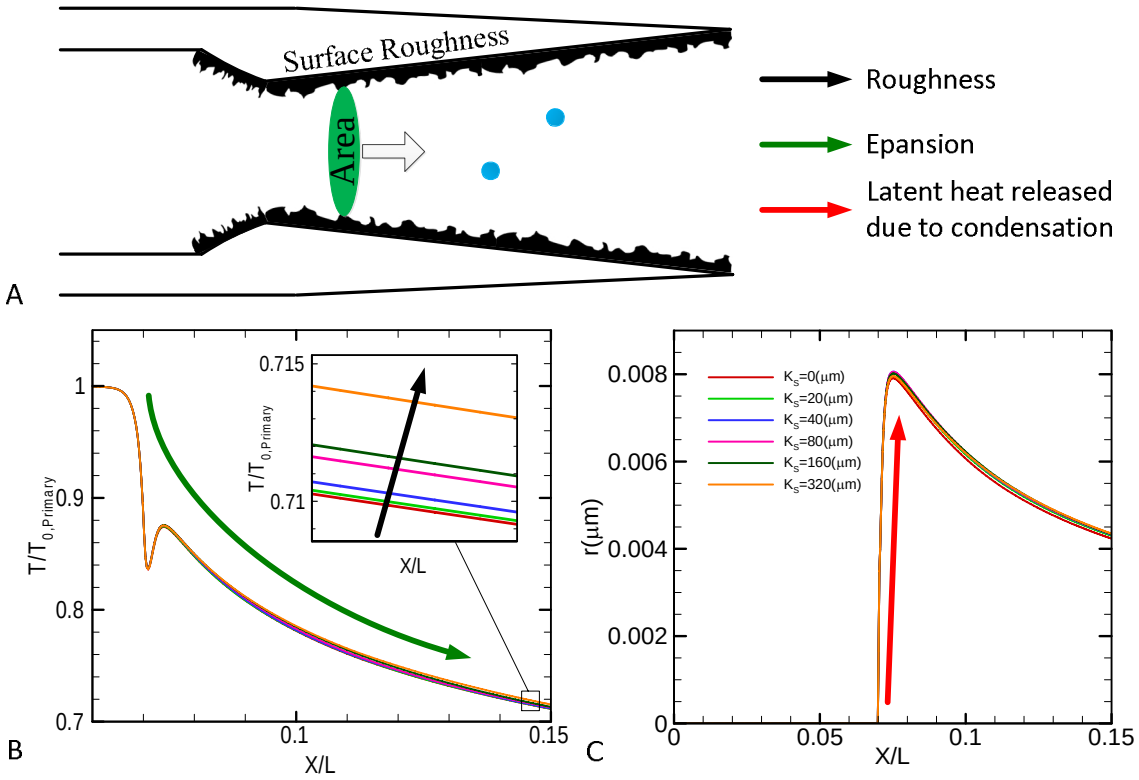

Fig.5 Effective parameters in the primary nozzle; A) schematic of the primary nozzle, B) temperature ratio of the centerline, and C) droplet average radius

To better understand the effect of roughness on flow as third factor, the area-weighted average values of mentioned properties are calculated at the primary nozzle exit (PNE) and is plotted in Fig.6. According to the Fanno Flow, the presence of friction in supersonic flow increases both pressure and temperature [35]. This can be seen in Fig.6 where the pressure rises from 2100Pa for smooth wall to 2500Pa for 320μm roughness height. The pressure curve shows that the pressure rising is intensified by increasing surface roughness, while temperature increase moderately. Furthermore, it is found that droplet average radius, droplet growth rate, and liquid mass fraction reduce with increasing surface roughness. This is because, the evaporation of droplets increases due to temperature increase. Although this variation seems to be slight, they strongly affect flow

condition ahead of shock chain and consequently ER of the ejector (see Fig.7).

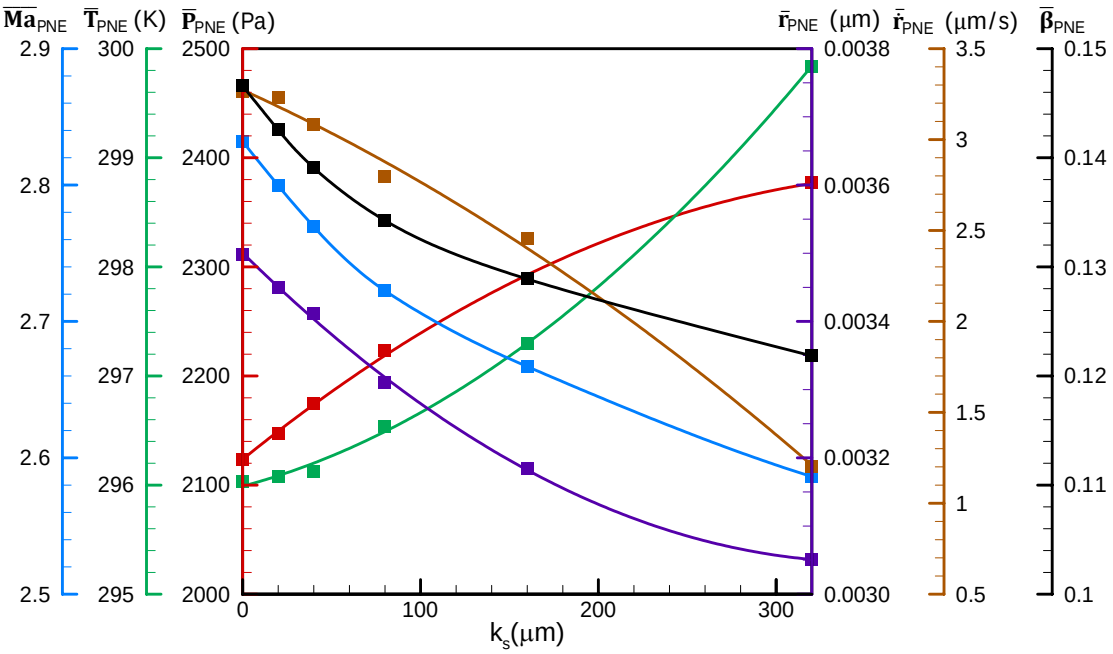

Fig.6. Average value of flow properties at the primary nozzle exit (PNE)

As can be seen in Fig.7(A), steam expansion continues in the mixing chamber and its pressure ratio drops to 0.2 which means that the mixing pressure is less than secondary flow pressure. From this point to the outlet of the ejector, the flow compressed and series of oblique aerodynamic shock is formed. However, the pressure rising becomes smoother in the constant area section, between $\frac{x}{L} = 0.42$ to $\frac{x}{L} = 0.56$. Fig.7(A) highlights that pressure pattern is similar for different roughness. But it causes variation as fallow:

- The section in which aerodynamic shock takes place moves upstream.
- Aerodynamic shock strength decreases at the beginning of the diffuser.
- The level of static pressure along the centerline has increased.

The pressure diagram clearly shows these changes, especially between $\frac{x}{L} = 0.26$ to $\frac{x}{L} = 0.34$, where the local valley has completely changed. Further, these changes can be seen in $T/T_{0,Primary}$ in Fig.7(B). Temperature distribution along with the ejector for different wall roughness is shown in Fig7.(B). Temperature curves generally have a downward, fluctuating, and upward pattern, respectively. Similar to the pressure diagram, it can be seen the temperature fluctuates due to the presence of the shock chain. Fig.7(B) indicates that the crest-trough interval of temperature

fluctuation decreases at the end of constant area section. However, the temperature increases along with diffuser.

To indicate the pressure and temperature distribution of whole flow field, their contour has been brought in Fig.8. These contours show that the effect of shock is reduced at the near-wall zone. It is also well observed that the lowest pressure occurs at the mixing chamber, which results in better suction of the secondary stream into the ejector. This figure clearly shows the pressure rising in constant area section. Furthermore, temperature contour shows that for smooth surface in the primary nozzle, a high-temperature zone emerges near the wall at the beginning of the diffuser. This value decrease by increment of roughness. Therefore, the temperature difference between the centerline and wall in diffuser decreases by increasing roughness.

Fig.7(C) shows the sensitivity of Mach number at the centerline. It is apparent that an abrupt increase in Mach number begins from the primary nozzle and reaches up to 1 at the nozzle throat. The continuous expansion causes the Mach number to increase until the shock chain occurs. Both pressure increase and shock chain from mixing chamber to end of the ejector cause to decreasing and fluctuating of Mach number, simultaneously. It is evident that the major effect of the pressure increase is to reduce the values of Mach number between $\frac{x}{L} = 0.3$ to $\frac{x}{L} = 0.9$. Fig.9 provides better vision of the distribution of Mach number throughout the ejector and shows the density of flow in the ejector. The maximum gradient of density occurs in the primary nozzle. The density of flow at the other zone of the ejector is in minimum value.

Fig.7(D) to (F) show the wet steam properties diagram. As can be seen, these properties severely increase around $\frac{x}{L} = 0.07$ where the nucleation occurs. At this point, the condensed nuclei are attached to each other and form droplets. As the nucleation rate reaches the maximum value, more nuclei join each other, and the droplet radius rapidly increases. Transmitted latent heat from droplets to steam phase increases flow pressure and consequently limits droplet growth rate (Fig.7(E)). Thereby, the droplet radius decreases. As can be seen, the behavior of wet steam parameters is in contrast to the pressure and temperature trend. In other words, the higher static temperature and pressure result in lower droplet average radius and liquid mass fraction. With increasing surface roughness, the liquid mass fraction emerging zone is significantly reduced. There is a similar trend for droplet average radius which is in good agreement with the temperature increase in the diffuser. Furthermore, the wet steam properties contours of simulations corresponding to different primary nozzle roughness are demonstrated in Fig.10 and 11. In

addition, Fig.10 indicates the only point in the ejector where the nucleation and consequently droplet growth rate appears. According to the simulation result in Fig.11, the near-wall zone of mixing chamber, constant area and diffuser have minimum value for droplet average radius, and liquid mass fraction. As seen in the temperature contour, the temperature rises from the center of the ejector to the walls and reaches its maximum at the side of the ejector wall. It seems that, this increase in temperature is the main factor in reducing the liquid mass fraction and the droplet average radius.

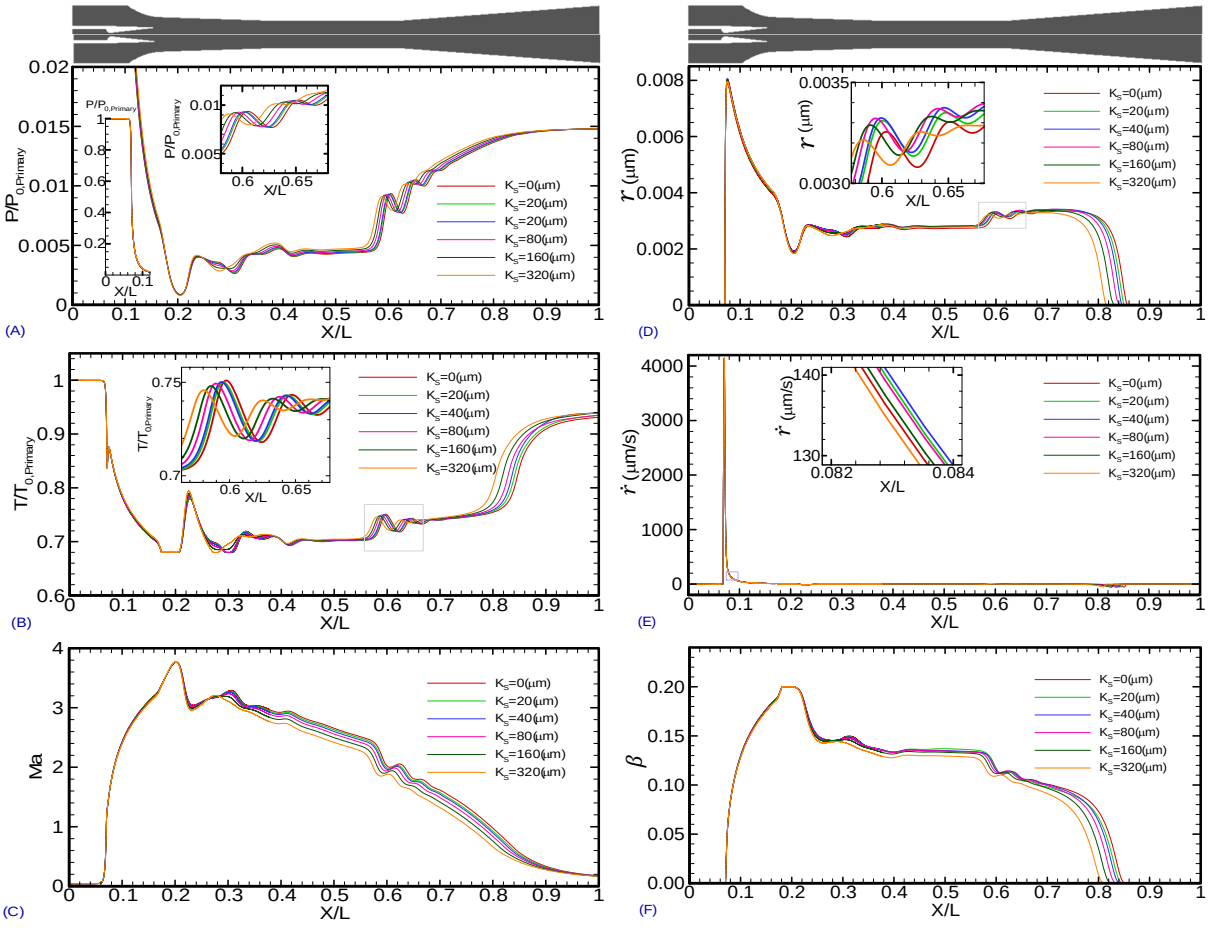

Fig.7. Distribution of different parameter on the centerline of the ejector by the increment of roughness in the primary nozzle A)pressure, B)temperature, C)Mach number, D)droplet average radius, E)droplet growth rate, and F)liquid mass fraction

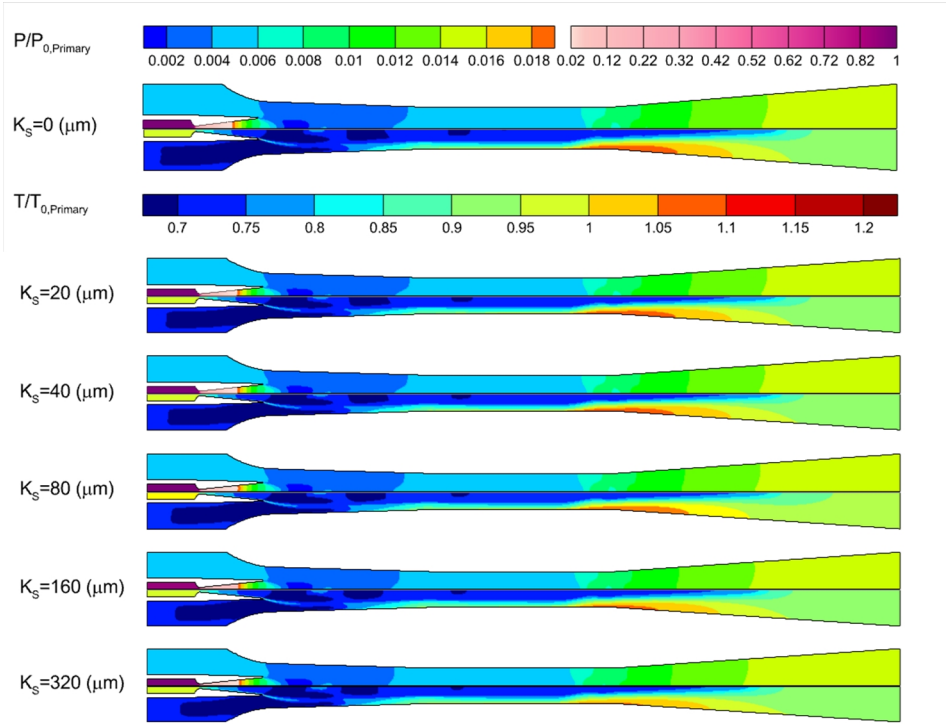

Fig.8. Contour of pressure (up) and temperature (down).

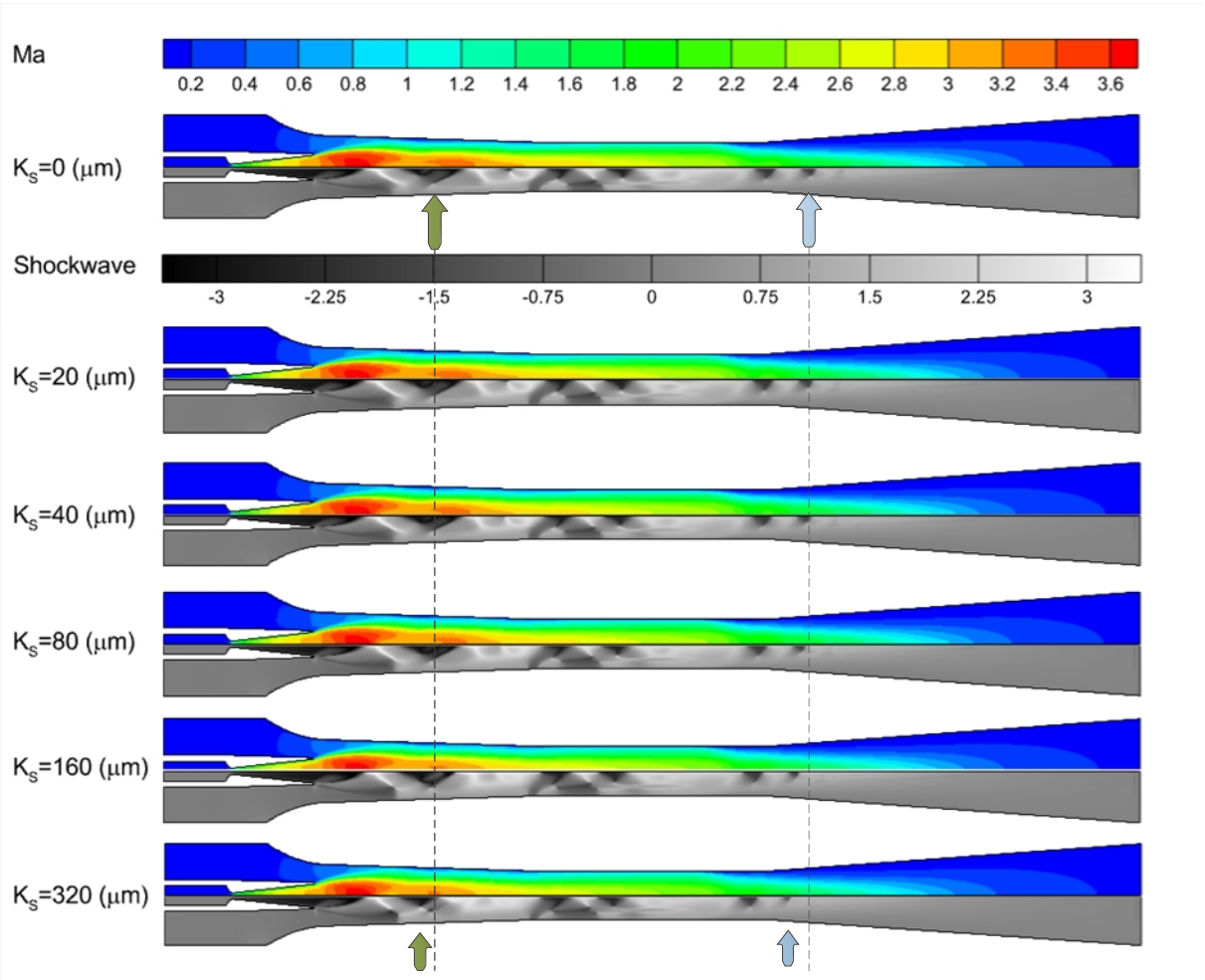

Fig.9. Contour of Mach number (up) and density/density gradient (down).

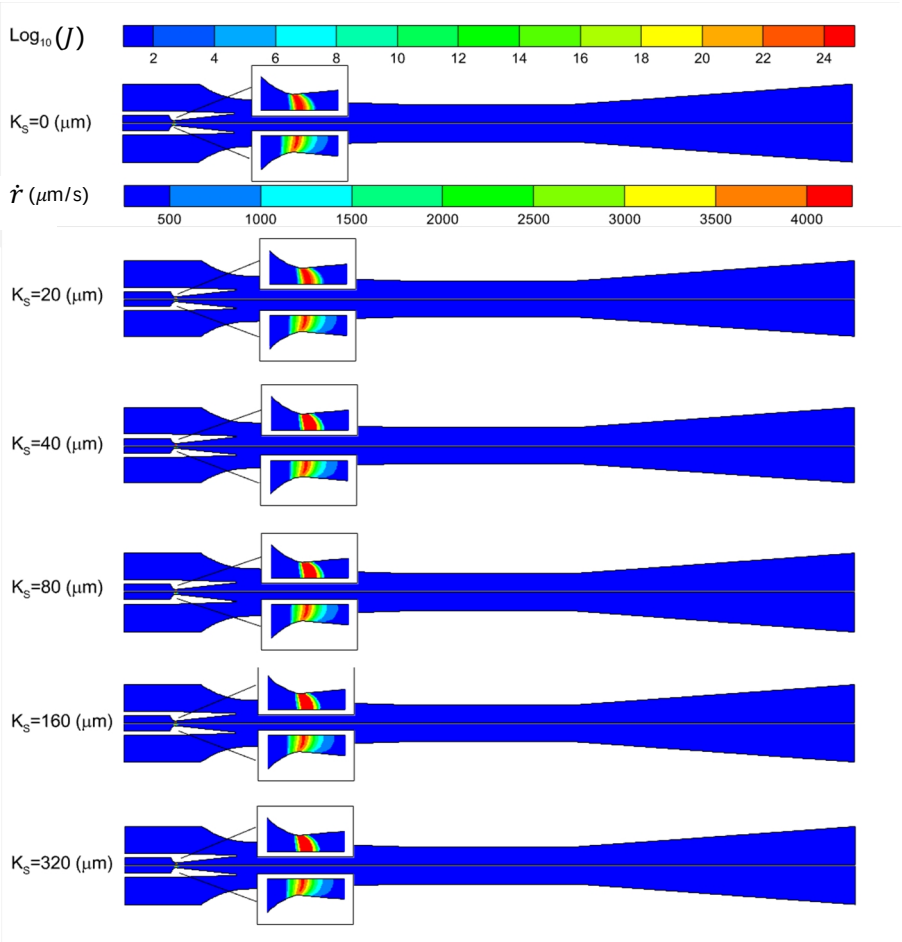

362

363 **Fig.10. Contour of droplet nucleation rate (up) and droplet growth rate (down)**

364

365

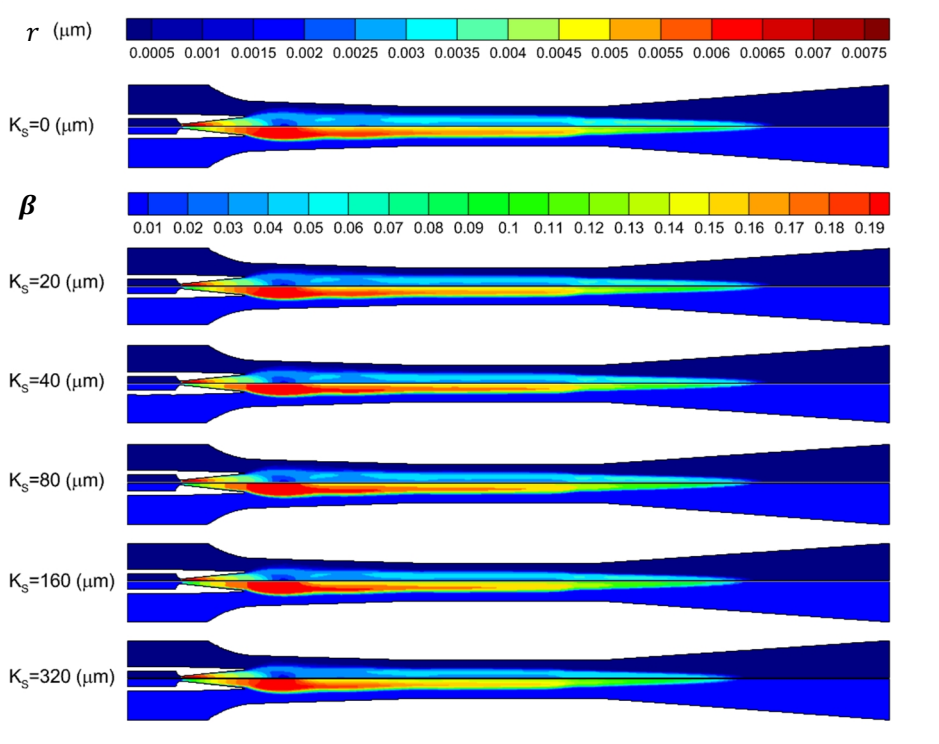

Fig.11. Contour of droplet average radius (up) and liquid mass fraction (down).

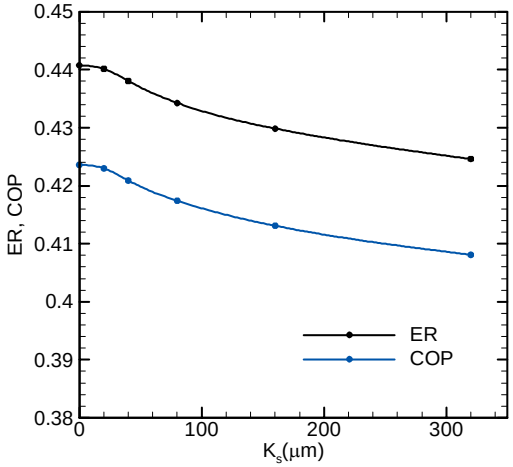

Fig.12. Effect of roughness height on ER and COP of refrigeration cycle

Fig.12 has been plotted to evaluate the influence of surface roughness on ER and COP of the ejector. As illustrated in the figure, the growth of the surface roughness in the range of 0 to $320\mu m$ results in reduction of ER and COP of the refrigeration cycle by 3.67% and 3.8%, respectively. This is because of more energy losses by the increment of surface roughness. Roughness height of

$20\mu m$ seems to be a critical point where the effect of wall roughness less than $20\mu m$ on ER can be neglected. Comparing Fig.12 with Fig.4C reveals that ER has a similar trend by an increase of backpressure and roughness. In fact, both of them lead to more loss of energy.

5. Conclusion

The effect of the primary nozzle surface roughness on the performance of wet steam ejectors with water as a working flow is analyzed. The practical aim of the present work is to better understand the correlation of wet steam properties with change in the surface roughness for possible promotion in the design and operation of wet steam ejectors. The most remarkable results from this study are as following:

- The pressure and temperature of flow increase due to roughness adding to the primary nozzle, while Mach number, droplet average radius, droplet growth rate, and liquid mass fraction have an opposite trend.
- Wall roughness has an influence on the passed flow through the ejector, wherein, roughness affects flow condition ahead of the primary nozzle and causes the section in which aerodynamic shock takes place to move upstream.
- Aerodynamic shock strength decreases at the beginning of the diffuser by increasing the wall roughness in the primary nozzle.
- Increment of primary nozzle surface roughness decreases ER and COP of the refrigeration cycle by 3.67% and 3.8%, respectively.

Therefore, designers and operators should be considered the roughness effects in design and operation of wet steam ejectors. Furthermore, the inner surface of the ejector should be monitored and controlled regularly.

6. References

[1] Edathol J, Brezgin D, Aronson K, Kim HD. Prediction of non-equilibrium homogeneous condensation in supersonic nozzle flows using Eulerian-Eulerian models. International journal of heat and mass transfer. 2020 May 1;152:119451. https://doi.org/10.1016/j.ijheatmasstransfer.2020.119451

[2] Yazdani S, Lakzian E. Numerical simulation and passive control of condensing flow through turbine blade by NVD Method Using Eulerian–Lagrangian Model. Computers & Mathematics with Applications. 2020 Jul 1;80(1):140-60. https://doi.org/10.1016/j.camwa.2020.03.007

[3] Ding H, Tian Y, Wen C, Wang C, Sun C. Polydispersed droplet spectrum and exergy analysis in wet steam flows using method of moments. Applied Thermal Engineering. 2021 Jan;182:116148. https://doi.org/10.1016/j.applthermaleng.2020.116148

[4] Dykas S, Wróblewski W. Single-and two-fluid models for steam condensing flow modeling. International Journal of Multiphase Flow. 2011 Nov 1;37(9):1245-53. https://doi.org/10.1016/j.ijmultiphaseflow.2011.05.008

[5] Alekseev RA, Gribin VG, Tishchenko AA, Gavrilov IY, Tishchenko VA, Popov VV. Application of PTV method for investigation of polydisperse wet steam flow. InJournal of Physics: Conference Series 2018 Nov 1 (Vol. 1128, No. 1, p. 012093). IOP Publishing. https://doi.org/10.1088/1742-6596/1128/1/012093

[6] Mahmoudian J, Mazzelli F, Milazzo A, Malpress R, Buttsworth DR. Experiments on water vapour condensation within supersonic nozzle flow generated by an impulse tunnel. International Journal of Multiphase Flow. 2021 Jan;134:103473. https://doi.org/10.1016/j.ijmultiphaseflow.2020.103473

[7] Milazzo A, Rocchetti A. Modelling of ejector chillers with steam and other working fluids. International Journal of Refrigeration. 2015 Sep 1;57:277-87. https://doi.org/10.1016/j.ijrefrig.2015.05.015

[8] Sharifi N, Boroomand M, Sharifi M. Numerical assessment of steam nucleation on thermodynamic performance of steam ejectors. Applied Thermal Engineering. 2013 Apr 15;52(2):449-59.https://doi.org/10.1016/j.applthermaleng.2012.12.003

[9] Aliabadi MA, Bahiraei M. Effect of water nano-droplet injection on steam ejector performance based on non-equilibrium spontaneous condensation: A droplet number study. Applied Thermal Engineering. 2021 Feb 5;184:116236. https://doi.org/10.1016/j.applthermaleng.2020.116236

[10] Li A, Yuen AC, Chen TB, Wang C, Liu H, Cao R, Yang W, Yeoh GH, Timchenko V. Computational study of wet steam flow to optimize steam ejector efficiency for potential fire

suppression application. Applied Sciences. 2019 Jan;9(7):1486. https://doi.org/10.3390/app9071486

[11] Zhang G, Dykas S, Li P, Li H, Wang J. Accurate condensing steam flow modeling in the ejector of the solar-driven refrigeration system. Energy. 2020 Dec 1;212:118690. https://doi.org/10.1016/j.energy.2020.118690

[12] Wang C, Wang L, Zhao H, Du Z, Ding Z. Effects of superheated steam on non-equilibrium condensation in ejector primary nozzle. International Journal of Refrigeration. 2016 Jul 1;67:214-26. https://doi.org/10.1016/j.ijrefrig.2016.02.022

[13] Wang X, Dong J, Li A, Lei H, Tu J. Numerical study of primary steam superheating effects on steam ejector flow and its pumping performance. Energy. 2014 Dec 15;78:205-11. https://doi.org/10.1016/j.energy.2014.10.004

[14] Ariafar K, Buttsworth D, Al-Doori G, Sharifi N. Mixing layer effects on the entrainment ratio in steam ejectors through ideal gas computational simulations. Energy. 2016 Jan 15;95:380-92.https://doi.org/10.1016/j.energy.2015.12.027

[15] Tang Y, Liu Z, Li Y, Wu H, Zhang X, Yang N. Visualization experimental study of the condensing flow regime in the transonic mixing process of desalination-oriented steam ejector. Energy Conversion and Management. 2019 Oct 1;197:111849. https://doi.org/10.1016/j.enconman.2019.111849

[16] Zou JJ, Zhou J, Lu HQ, Hu Y. Experimental investigation on starting process of supersonic single-stage air ejector. Journal of thermal science. 2012 Aug 1;21(4):348-53. https://doi.org/10.1007/s11630-012-0554-1

[17] Foroozesh F, Khoshnevis AB, Lakzian E. Improvement of the wet steam ejector performance in a refrigeration cycle via changing the ejector geometry by a novel EEC (Entropy generation, Entrainment ratio, and Coefficient of performance) method. International Journal of Refrigeration. 2020 Feb 1;110:248-61. https://doi.org/10.1016/j.ijrefrig.2019.11.006

[18] Dong J, Hu Q, Yu M, Han Z, Cui W, Liang D, Ma H, Pan X. Numerical investigation on the influence of mixing chamber length on steam ejector performance. Applied Thermal Engineering. 2020 Jun 25;174:115204. https://doi.org/10.1016/j.applthermaleng.2020.115204

[19] Zhang G, Dykas S, Yang S, Zhang X, Li H, Wang J. Optimization of the primary nozzle based on a modified condensation model in a steam ejector. Applied Thermal Engineering. 2020 May 5;171:115090. https://doi.org/10.1016/j.applthermaleng.2020.115090

[20] Wang C, Wang L, Zou T, Zhang H. Influences of area ratio and surface roughness on homogeneous condensation in ejector primary nozzle. Energy Conversion and Management. 2017 Oct 1;149:168-74.https://doi.org/10.1016/j.enconman.2017.07.025

[21] Mahmoudian J, Mazzelli F, Milazzo A, Rocchetti A. Experimental and numerical activity on a prototype ejector chiller. InJournal of Physics: Conference Series 2020 Aug 1 (Vol. 1599, No. 1, p. 012056). IOP Publishing. https://doi:10.1088/1742-6596/1599/1/012056

[22] Zhang H, Wang L, Jia L, Wang X. Assessment and prediction of component efficiencies in supersonic ejector with friction losses. Applied Thermal Engineering. 2018 Jan 25;129:618-27. https://doi.org/10.1016/j.applthermaleng.2017.10.054

[23] Zhang H, Wang L, Jia L, Zhao H, Wang C. Influence investigation of friction on supersonic ejector performance. International Journal of Refrigeration. 2018 Jan 1;85:229-39. https://doi.org/10.1016/j.ijrefrig.2017.09.028

[24] Yang Y, Du W, Ma T, Lin W, Cong M, Yang H, Yu Z. Numerical studies on ejector structure optimization and performance prediction based on a novel pressure drop model for proton exchange membrane fuel cell anode. International Journal of Hydrogen Energy. 2020 Sep 3;45(43):23343-52. https://doi.org/10.1016/j.ijhydene.2020.06.068

[25] Brezgin DV, Aronson KE, Mazzelli F, Milazzo A. The surface roughness effect on the performance of supersonic ejectors. Thermophysics and Aeromechanics. 2017 Jul;24(4):553-61.https://doi.org/10.1134/S0869864317040060

[26] Pillai A, Prasad BV. Effect of wall surface roughness on condensation shock. International Journal of Thermal Sciences. 2018 Oct 1;132:435-45. https://doi.org/10.1016/j.ijthermalsci.2018.06.028

[27] Han X, Liu X, Yuan Y, Han Z. Effect of blade surface roughness on condensation process in a stator cascade. International Journal of Numerical Methods for Heat & Fluid Flow. 2019 Dec 7. https://doi.org/10.1108/HFF-10-2019-0736

[28] Ding H, Li Y, Lakzian E, Wen C, Wang C. Entropy generation and exergy destruction in condensing steam flow through turbine blade with surface roughness. Energy Conversion and Management. 2019 Sep 15;196:1089-104. https://doi.org/10.1016/j.enconman.2019.06.066

[29] Esfe HB, Kermani MJ, Avval MS. Effects of surface roughness on deviation angle and performance losses in wet steam turbines. Applied Thermal Engineering. 2015 Nov 5;90:158-73. https://doi.org/10.1016/j.applthermaleng.2015.07.007

[30] Ruangtrakoon N, Aphornratana S, Sriveerakul T. Experimental studies of a steam jet refrigeration cycle: effect of the primary nozzle geometries to system performance. Experimental Thermal and Fluid Science. 2011 May 1;35(4):676-83. https://doi.org/10.1016/j.expthermflusci.2011.01.001

[31] Ebrahimi-Fizik A, Lakzian E, Hashemian A. Numerical investigation of wet inflow in steam turbine cascades using NURBS-based mesh generation method. International Communications in Heat and Mass Transfer. 2020 Nov 1;118:104812. https://doi.org/10.1016/j.icheatmasstransfer.2020.104812

[32] Mazzelli F, Little AB, Garimella S, Bartosiewicz Y. Computational and experimental analysis of supersonic air ejector: Turbulence modeling and assessment of 3D effects. International Journal of Heat and Fluid Flow. 2015 Dec 1;56:305-16. https://doi.org/10.1016/j.ijheatfluidflow.2015.08.003

[33] Senguttuvan S, Lee JC. Numerical study of wet-steam flow in Moore nozzles. Journal of Mechanical Science and Technology. 2019 Oct;33(10):4823-30. https://doi.org/10.1007/s12206-019-0923-8

[34] Kermani MJ, Gerber AG. A general formula for the evaluation of thermodynamic and aerodynamic losses in nucleating steam flow. International journal of heat and mass transfer. 2003 Aug 1;46(17):3265-78. https://doi.org/10.1016/S0017-9310(03)00096-6.

[35] F.M. White, FLUID MECHANICS, Eighth Edition, McGraw-Hill Education, 2016.